Available online at www.sciencedirect.com
SCIENCE DIRECT®
Atmospheric Environment 39 (2005) 4969–4982
ATMOSPHERIC ENVIRONMENT
www.elsevier.com/locate/atmosenv

Hygroscopic properties of an organic-laden aerosol

William C. Malm[a,*], Derek E. Day[b], Sonia M. Kreidenweis[c], Jeffrey L. Collett Jr.[c], Christian Carrico[c], Gavin McMeeking[c], Taehyoung Lee[c]

[a]*National Park Service, Cooperative Institute for Research in the Atmosphere, Colorado State University, Fort Collins, CO 80523-1375, USA*
[b]*Cooperative Institute for Research in the Atmosphere, Colorado State University, Fort Collins, CO 80523-1375, USA*
[c]*Department of Atmospheric Science, Colorado State University, Fort Collins, CO 80523-1371, USA*

Received 28 January 2005; accepted 4 May 2005

Abstract

Observation and appreciation of scenic landscape features, airport runway visibility, and the earth's radiation balance are all dependent on the radiative properties of the atmosphere, which in turn are dependent on the scattering and absorption characteristics of ambient aerosols. Atmospheric scattering and, to a lesser degree, absorption characteristics are highly dependent on the amount of water vapor absorbed by aerosols under ambient relative humidity (RH) conditions. Water vapor absorptive properties of inorganic aerosols have been extensively measured and modeled; however, hygroscopic properties of organic aerosols are less understood, especially as they occur in the ambient atmosphere. Therefore, an aerosol characterization study was conceived and implemented at Yosemite National Park, which is highly impacted by carbonaceous aerosols. The overall objective of the study was to characterize the physical, chemical, and optical properties of a carbon-dominated aerosol, including the ratio of total organic matter weight to organic carbon, organic mass scattering efficiencies, and the hygroscopic characteristics of a carbon-laden ambient aerosol. The study was conducted during July, August, and the first week of September at Turtleback Dome on the south rim of the entrance to Yosemite Valley. The ratio of the scattering coefficient at some RH divided by the scattering coefficient at some minimum RH ($f(\mathrm{RH}) = b_{\mathrm{scat}}(\mathrm{RH})/b_{\mathrm{scat}}(\mathrm{RH_{min}})$) was measured over a wide range of RHs. $f(85<\mathrm{RH}<90)$ decreased from about 2.0 to <1.2 as the organic carbon mass ($\mathrm{OMC}/(\mathrm{NH_4})_2(\mathrm{SO_4})$) ratio increased from a low of 0.57 to 11.15, implying that the $f(\mathrm{RH})$ associated with organics is small, possibly on the order of 1.1 or less. Furthermore, modeling $f(\mathrm{RH})$ as a function of RH suggested that ambient organic mass aerosols may be weakly hygroscopic with an $f(\mathrm{RH})$ at RH = 85–90% of about 1.1.

Keywords: Hygroscopicity; Aerosol scattering; Organic optical properties; Mass scattering efficiency; Particle size distributions

1. Introduction

Radiative properties of the atmosphere are affected by scattering and absorption characteristics of aerosols. Understanding these properties is essential to understanding the earth's radiation balance and the ability to

*Corresponding author. Tel.: +1 970 491 8292; fax: +1 970 491 8598.
E-mail address: malm@cira.colostate.edu (W.C. Malm).

1352-2310/$ - see front matter © 2005 Elsevier Ltd. All rights reserved.
doi:10.1016/j.atmosenv.2005.05.014

see and appreciate the many scenic vistas found throughout the world. Atmospheric scattering and, to a lesser degree, absorption characteristics are highly dependent on the amount of water vapor absorbed by aerosols under ambient relative humidity (RH) conditions. The water vapor absorptive properties of inorganic aerosols have been extensively measured, and a number of equilibrium models describing these properties as a function of inorganic ion mixtures have been developed (Kim et al., 1993; Clegg et al., 1998a, b; Nenes et al., 1998). Although recent laboratory measurements of hygroscopic properties of organic aerosols have been carried out, less is known about the hygroscopic characteristics of ambient organic aerosols or mixtures of inorganic and organic species as they occur in the ambient atmosphere.

Over the past few years, the number of measurements of laboratory and ambient organic aerosol hygroscopicity has increased. Cocker et al. (2001) have summarized tandem differential mobility analyzer (TDMA) data up to the year 2001. Many of these studies report on aerosol growth measurements (D/D_o) without interpreting the results in the context of how much growth or growth modification can be attributed to varying concentrations of aerosols species. Virkkula et al. (1999) did report a growth factor for secondary organic aerosols of 1.1 at about 85% RH. Brooks et al. (2004) and Prenni et al. (2003) carried out laboratory studies addressing the ability of mixtures of inorganic and organic aerosols to absorb water. They found that mixing organic aerosols with inorganic species caused the deliquescence point associated with the pure inorganic species to be slightly depressed and that, to within the uncertainty of the measurements, the water vapor uptake of the mixtures is consistent with the measured water uptake observed for each species measured independently. Ansari and Pandis (2000) report that secondary organic aerosols can account for about 20% of the absorbed water when they are approximately 30% of the fine mass. Gysel et al. (2004) report that the growth factor at 90% RH for a "less hydrophilic" fraction of water soluble organics (WSO), which makes up most of the WSO, was between 1.08 and 1.17. Busch et al. (2002) report that the hygroscopic growth of aerosols in the Lindenberg Aerosol Characterization Experiment was characterized by more and less hygroscopic aerosols. The less hygroscopic group, presumably organics, had growth factors of about 1.1 at 90% RH.

While the TDMA is used to measure D/D_o as a function of RH for a given particle size, measurements of the RH enhancement factor, the ratio of the scattering coefficient at some RH divided by the scattering coefficient at some minimum RH ($f(\mathrm{RH}) = b_{\mathrm{scat}}(\mathrm{RH})/b_{\mathrm{scat}}(\mathrm{RH_{min}})$), are integrated measurements of growth associated with the full-size distribution of particles entering the nephelometer. Measurements of this type were pioneered by Covert et al. (1979).

Malm and Day (2001) and Malm et al. (2000, 2003) reported on measurements carried out at Great Smoky Mountains, Grand Canyon, and Big Bend national parks. The f(RH) function at Great Smoky and Big Bend national parks for the most part suggested that the aerosols retained water down to RHs as low as 20%, which was consistent with sulfate aerosols that were not fully neutralized, while at Grand Canyon the f(RH) function did not increase beyond one until about 40–50% RH.

A number of scattering models were used in an attempt to reproduce measured f(RH) curves. At Great Smoky Mountains, both internally and externally mixed aerosol models were used, assuming the measured sulfate ion was fully neutralized and assuming variable degrees of neutralization corresponding to the measured ammonium ion concentrations and with and without accounting for sampling-period-to-sampling-period shifts in size distribution (Malm et al., 2000). Scattering coefficient predictions as a function of RH were most sensitive to the assumptions regarding sulfate ammoniation, while assumptions concerning mixing were $<10\%$ on the average. On the average, 63% of the fine aerosol mass was sulfates and 25% was organics. During the Grand Canyon study, 31% and 44% of the fine mass were associated with sulfates and organics, respectively. However, at Grand Canyon assumptions concerning sulfate ammoniation were not necessary to successfully model f(RH). The results of both the Grand Canyon and Great Smoky Mountains studies suggested that organic aerosols were weakly hygroscopic or non-hygroscopic.

At Big Bend National Park sulfates and organics made up 51% and 21% of the fine mass concentrations, respectively. Four general types of f(RH) curves were observed: deliquescent and crystallization behaviors, continuous growth from about 25–30% RH where the aerosol was apparently dry at the minimum RH, and continuous growth from 25% to 30% RH but where the aerosol retained water at the minimum RHs. Dry scattering as a function of RH was compared to modeled estimates of scattering that incorporated aerosol species concentrations, mass size distributions, and estimates of aerosol growth based on three equilibrium models. Dry mass scattering efficiencies of ammoniated sulfate varied from a low of $2.42\,\mathrm{m^2\,g^{-1}}$ to a maximum of $4.06\,\mathrm{m^2\,g^{-1}}$, with an average of $3.15\,\mathrm{m^2\,g^{-1}}$. The lowest efficiencies occurred on the lowest mass concentration days, while the highest efficiencies corresponded to the highest mass loadings. The assumption that only inorganic species were hygroscopic was sufficient, to within the uncertainty of the measurement, to account for the measured increase in f(RH) as a function of RH. The average difference

between measured and modeled f(RH) above 35% RH was on the order of 1%.

In all these measurement programs, organic mass concentrations were never the dominant species and assessing their hygroscopicity, beyond stating that they are weakly to not hygroscopic, has proven to be difficult. Therefore, an aerosol characterization study was conceived and implemented at Yosemite National Park, which is highly impacted by carbonaceous aerosols. On the average, carbonaceous material contributes about 50–60% of the fine ($<2.5\,\mu m$) aerosols, and during the fall season that percentage can be in excess of 80%. The overall objective of the study was to characterize the physical, chemical, and optical properties of a carbon-dominated aerosol, including the ratio of total organic matter weight to organic carbon, organic carbon mass (OMC) scattering efficiencies, and the hygroscopic characteristics of a carbon-laden ambient aerosol. The study was conducted during July, August, and the first week of September at Turtleback Dome on the south rim of the entrance to the Yosemite Valley Interagency Monitoring of Protected Visual Environments (IMPROVE) monitoring site at longitude 119.70°W, latitude 37.71°N, elevation 1615 m. The overall study is described fully by Carrico et al. (2005). This paper will focus on assessing the hygroscopic characteristics, as represented by f(RH) measurements, of an organic-laden ambient aerosol.

2. Methods

The variables and instruments used to make the measurements are summarized in Table 1, which also includes a reference for each measurement methodology. The details of the measurement methodologies can be found in each of the references and will not be discussed in detail here.

2.1. Particulate measurements

The IMPROVE monitoring system (Malm et al., 1994) was used during this study. The analytic analysis is carried out under a well-defined protocol (http://vista.cira.colostate.edu/improve/Publications/SOPs/ucdavis_sops/sop301.pdf). Basically, it consists of three modules or channels. Each channel has its own filter and sample inlet; however, a single computer controls all channels. Typically, the channels are referred to as A (from which aerosol gravimetric mass and elements Na–Pb are measured), B (from which ions are measured), and C (analyzed for organic (OC) and light absorbing carbon (LAC) by thermal optical reflectance (TOR)) (Chow et al., 1993). Samples were collected for 24 h beginning at 0800 PST.

A URG sampling system was also employed during the Yosemite study. It consisted of a 2.5 μm cyclone, two denuders coated with Na_2CO_3 and H_3PO_3 to remove nitric acid and ammonia gas, respectively, a Teflo® primary filter for particle collection, and a nylon backup filter to collect any nitrate which escaped from the primary filter. Filter extracts were analyzed by ion chromatography for major ions including SO_4^{2-}, NO_3^-, Cl^-, Na^+, K^+, Ca^{2+}, Mg^{2+}, NH_4^+, and oxalate. Extracts from the two denuders were analyzed to obtain HNO_3, NH_3, SO_2, and oxalic acid gas phase concentrations.

The micro-orifice uniform deposit impactor (MOUDI) sampling system is designed to selectively collect particles in nine discrete size ranges (>18.0, 10.0–18.0, 5.6–10.0, 3.2–5.6, 1.8–3.2, 1.0–1.8, 0.56–1.0, 0.32–0.56, and 0.18–0.32 μm) and includes an after-filter which collects all those aerosols <0.18 μm. Coated aluminum foil was used as a substrate while the after-filter was Teflo®. Analyses of sample extracts were done by ion chromatography for major anions (SO_4^{2-}, NO_3^-, Cl^-) and major cations (NH_4^+, Na^+, Ca^{2+}, K^+).

The particle-into-liquid sampler (PILS) (Orsini et al., 2003) was operated continuously during the Yosemite study to obtain the concentration of major ions (Na^+, K^+, Ca^{2+}, Mg^{2+}, Cl^-, NO_3^-, and SO_4^{2-}) with a time resolution of 15 min. This system introduces atmospheric particles into a supersaturated environment by mixing the airflow with 100 °C steam, which grows the particles large enough to be collected by an impactor. The droplets are washed off the impactor and collected in a flowing liquid stream that is analyzed by ion chromatography. An internal LiBr standard is used to account for dilution by condensed steam.

A Rupprecht and Patashnick (R&P) model 5400 (Rupprecht et al., 1995) ambient carbon particulate monitor operated with a 2.5 μm size cut inlet was used to measure aerosol total carbon (TC) while a two-channel aethalometer was used to measure aerosol absorption at two wavelengths. This instrument was also run with a 2.5 μm cyclone in front of the sample line but with a 5-min measurement frequency.

2.2. Aerosol particle size

Ambient aerosol was sampled through a flow splitter to deliver a common aerosol sample to the particle sizing instrumentation. Dry size distributions were measured with an electrical mobility technique ($40\,nm < D < 850\,nm$ using TSI Inc., models 3081 and 3010), and an optical sizing technique ($0.1 < D < 2\,\mu m$ using Particle Measuring Systems, Inc., LASAIR 1002 and 1003). Aerosol drying was accomplished using Nafion® membrane driers (Perma Pure Inc.). Examination of the overlapping regions for these measurements yields information on

Table 1
Summary of SEQ CHAPTER chemical analyses

Sampler/instrument and size cut	Variable measured	Substrate	Denuder	Time	Analytical technique	Reference
IMPROVE $PM_{2.5}$ Chan A	Elements, mass	Teflon	None	24 h	XRF, gravimetric	Malm et al. (1994)
IMPROVE $PM_{2.5}$ Chan B	Anions	Nylon	Na_2CO_3	24 h	Ion chromatography	Malm et al. (1994)
IMPROVE $PM_{2.5}$ Chan C	Carbon	Quartz	None	24 h	TOR	Malm et al. (1994)
IMPROVE PM_{10} Chan A	Elements, mass	Teflon	None	24 h	XRF, gravimetric	Malm et al. (1994)
IMPROVE PM_{10} Chan B	Anions	Nylon	Na_2CO_3	24 h	Ion chromatography	Malm et al. (1994)
IMPROVE PM_{10} Chan C	Carbon	Quartz	None	24 h	TOR	Malm et al. (1994)
URG $PM_{2.5}$	Ions	Teflo primary nylon backup	Na_2CO_3/ H_3PO_3	24 and 6 h intensives	Ion chromatography	Lee et al. (2004)
MOUDI multi-stage impactor	Ions	Aluminum foil Teflo after-filter	None	24 and 12 h intensives	Ion chromatography	Marple et al. (1991)
PILS $PM_{2.5}$	Ions	None	$NaCO_3$/ H_3PO_4	15 min	Ion chromatography	Orsini et al. (2003)
SEM $PM_{2.5}$	Particle morphology and atomic weight	Copper mesh grids with carbon films	None	15 min	Scanning electron microscope and EDX	Laskin et al. (2003)
R&P $PM_{2.5}$	Total carbon	Stainless-steel impactor	None	1 h	Thermal desorption	Rupprecht et al. (1995)
Aethalometer $PM_{2.5}$	Black carbon	Quartz	None	5 min	Light absorption	Hansen et al. (1984)
PM_{10} nephelometer (ambient)	PM_{10} b_{sp}	NA	NA	2 min	Optical scattering	Molenar (1997)
$PM_{2.5}$ nephelometer (ambient)	$PM_{2.5}$ b_{sp}	NA	NA	2 min	Optical scattering	Day and Malm (2001)
$PM_{2.5}$ nephelometer (dry)	$PM_{2.5}$ b_{sp}	NA	NA	2 min	Optical scattering	Day and Malm (2001)
Transmissometer (ambient)	b_{ext}	NA	NA	2 min	Optical extinction	Molenar et al. (1989)
Humidograph $PM_{2.5}$ under controlled RH conditions	f(RH)	NA	NA	2 min	Optical scattering	Day and Malm (2001)
Tandem differential mobility analyzer (HTDMA)	D/D_o(RH)	NA	NA	15 min	Electric mobility	Rader and McMurry (1986)
Electric mobility analyzer	Number size dist. (0.04–0.85 μm)	NA	NA	15 min	Electric mobility	Armendariz and Leith (2002)
Optical particle counter	Number size dist. (0.1–2.0 μm)	NA	NA	15 min	Light scattering	Hering and McMurry (1991)

the refractive index (Hand and Kreidenweis, 2002; Hand et al., 2002).

2.3. Optical measurements

An Optec, Inc., LPV-2 instrument was used to measure extinction. Its use in remote locations such as national parks is discussed by Molenar et al. (1989), while its use in urban settings is presented by Dietrich et al. (1989). Careful operation of the transmissometer (daily cleaning of optics and pre- and post-calibrations) should result in extinction measurements with an accuracy of about 10% (Molenar et al., 1989).

Optec NGN-2 integrating nephelometers were operated in various configurations (Malm et al., 1994; Molenar, 1997; Day et al., 2000). A set of two nephelometers were operated in the open-air configuration according to standard IMPROVE protocols and another set of two were operated with a Bendix-240

(Chan and Lippman, 1977) cyclone inlet with a 2.5 μm cutpoint. The Optec instruments have an effective wavelength sensitivity of 550 nm (http://vista.cira.colostate.edu/improve/Publications/GrayLit/gray_literature.htm).

The aerosol light scattering coefficient measured as a function of RH was determined using two Radiance Research M903 nephelometers, which measure scattering at an effective wavelength of 530 nm. A dry, or reference, nephelometer was fitted with an inlet consisting of a bundle of ten Perma Pure Nafion® dryers operated in parallel to precondition the aerosol to about 5–10% RH (Day and Malm, 2001). This system of dryers was further fitted with a 2.5 μm cyclone inlet. The second nephelometer sampled from two RH preconditioners operated in series. The purpose was to either precondition the aerosol to approximately 80% RH in the first humidification system and dry the aerosol in the second (crystallization curve), or dry the aerosol in the first system and humidify in the second, allowing for measurement of the deliquescent $f(RH)$ curve. This sampling train was also fitted with a 2.5 μm cyclone. An RH scan from a low of about 15% to >95% took on the order of 2–3 h.

Temperature changes in the sampling plumbing can cause unwanted and unknown RH changes. Rotronic MP-100F combination RH/temperature sensors were used to measure these variables throughout the system. The reported accuracy of the RH sensor is ±2% (Rotronic Instrument Corp., 1998).

3. Summary of the aerosol data set

Malm et al. (2005) discuss the harmony between these various measurement technologies as well as the implied chemical composition of various aerosol species. It was found that the 24-h bulk measurements agreed well with each other, with the semi-continuous measurements typically being biased low compared to the 24-h average data. Semi-continuous sulfate data were approximately 0.15 $\mu g\,m^{-3}$ lower than the bulk data, while the nitrate data were biased both in an additive and multiplicative way. The R&P TC data compared least favorably with the bulk measurements in that, on the average, they over-predicted when the TC concentrations were low, and under-predicted when TC mass concentrations were elevated. On the average, R&P-derived carbon was 40% higher than IMPROVE/TOR carbon. Therefore, when any data collected with semi-continuous monitors were used, the data were normalized on a 24-h basis to concentrations derived from the URG and IMPROVE sampling systems (Malm et al., 2005).

Analysis of the MOUDI data showed that, on the average, ionic species in the fine mode (0.0–2.5 μm) are made up of primarily ammonium sulfate with about 6% ammonium nitrate, 2% sodium chloride, and 9% excess cation mass. It was further shown that fine nitrate (<2.5 μm) was actually the fine tail of coarse mode nitrate that was typically in the form of $NaNO_3$. The coarse mode ionic mass is primarily in the form of $NaNO_3$, NaCl, and soil-related nitrate products. It was further shown that, in most cases, fine mass closure was achieved with an organic mass to organic carbon ratio of 1.8 rather than the more typically

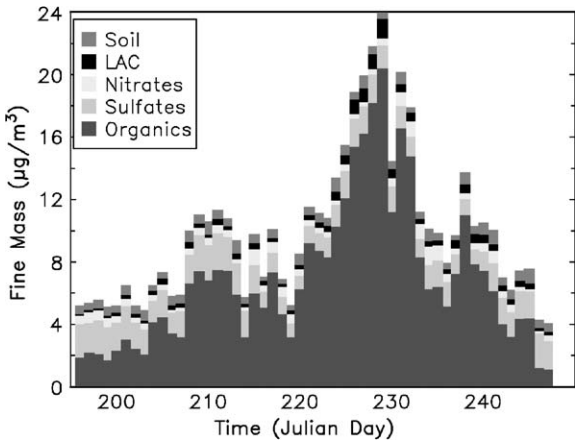

Fig. 1. Temporal plot of 24-h average of the five major aerosol species.

Table 2
Statistical summary of fifty-two 24 h average aerosol species concentrations

Variable ($\mu g\,m^{-3}$)	Mean	Std. Dev.	Minimum	Maximum
Gravimetric mass	9.61	4.47	4.06	23.35
Reconstructed mass	9.85	4.74	4.09	23.86
Ammonium sulfate	1.59 (16)	0.41	0.84	2.38
Sodium nitrate	0.48 (5)	0.23	0.16	1.20
Organics	6.81 (69)	4.59	1.08	20.41
Light-absorbing carbon	0.38 (4)	0.22	0.10	1.23
Soil	0.59 (6)	0.16	0.29	0.94

used 1.4 (United States Environmental Protection Agency, 2003).

Fig. 1 shows a stacked bar plot of 24-h fine aerosol species mass concentrations as a function of time, while Table 2 is a statistical summary of these species. Sulfate is interpreted as ammonium sulfate, nitrate as sodium nitrate, OMC as $1.8 \times$ OC, and soil mass as the oxides of soil-related elements (Malm et al., 2005). Reconstructed mass is the sum of these species including LAC. Also, shown parenthetically in Table 2 is the fraction that each species contributes to reconstructed fine mass. On an average basis, OMC made up 69% of the mass while ammonium sulfate was a distant second at 16%. All other species concentrations contributed to fine mass at $<6\%$. The maximum 24-h OMC mass concentration is $20.41\,\mu g\,m^{-3}$ or 85% of the measured fine mass. There are two elevated concentration episodes, one centered on Julian day 210, the other around Julian day 228, both of which are dominated by carbonaceous aerosol mass.

4. Summary of particle number size distribution measurements

A detailed discussion of aerosol number size distribution measurements can be found in McMeeking et al. (2005). Aerosol size distributions in the range between $0.04 < D_p < 2\,\mu m$ for "dry" measurements were derived by merging differential mobility analyzer (DMA) and optical particle counter size distribution measurements following the procedure given by Knutson and Lioy (1989). Table 3 summarizes, among other variables, the geometric mean diameter and standard deviation of the derived volume size distributions. The geometric mean diameter is $0.33\,\mu m$ with a maximum mean size of $0.43\,\mu m$ and minimum of $0.19\,\mu m$, while the geometric standard deviation varies between 1.51 and 2.38 with a mean of 1.88. McMeeking et al. (2005) show that as the volume (mass) increases, the geometric mean diameter tends to increase while the volume distributions become more narrow (σ_g decreases).

5. Summary of optical measurements

In the paper by Malm et al. (2005), the optical measurements are also summarized. They show that the difference between average dry and ambient scattering is only on the order of about $2.63\,Mm^{-1}$, which is well within the uncertainty of the measurements. This small difference is consistent with the low average RH and little hygroscopic growth at ambient humidities. Furthermore, the difference between PM_{10} and $PM_{2.5}$ scattering is small at $1.46\,Mm^{-1}$, which again is within the nephelometer stated uncertainties. It is known that the PM_{10} nephelometer underestimates coarse particle scattering by about a factor of 2; therefore, average coarse particle scattering would be about $3\,Mm^{-1}$ (http://vista.cira.colostate.edu/improve/Publications/GrayLit/014_AerosolByNeph/AerosolbyNeph.pdf). Differencing total extinction and measured PM scattering plus $1.5\,Mm^{-1}$ to account for the nephelometer large particle truncation error yields $9.7\,Mm^{-1}$ of absorption. Therefore, based on optical measurements, 75% of extinction is dry fine particle scattering, 6% is coarse particle scattering, 14% is coarse and fine absorption, and 5% is scattering due to absorbed water. Only the scattering derived from the "dry" and artificially modified RH nephelometers will be used in the following discussions.

6. Modeling atmospheric scattering

It is the DMA number size distributions that are used to model scattering as a function of RH and its ratio to dry scattering. To assess the ability of optical models to accurately predict scattering from size distribution

Table 3
Statistical summary of volume size distribution measurements, volume-weighted index of refraction, derived mass scattering and absorption efficiencies, modeled and measured scattering, and absorption

Variable	Mean	Std. Dev.	Minimum	Maximum	N
Geometric mean diameter (μm)	0.33	0.04	0.19	0.43	939
Geometric Std. Dev.	1.88	0.17	1.51	2.38	939
Real index of refraction	1.56	0.01	1.55	1.59	1032
Complex index of refraction	0.02	0.01	0.01	0.04	1032
Mass scattering efficiency ($m^2\,g^{-1}$)	4.49	0.76	2.28	5.96	939
Mass absorption efficiency ($m^2\,g^{-1}$)	0.46	0.12	0.16	0.90	939
Derived b_{sp} ($M\,m^{-1}$)	48.84	32.47	5.98	202.50	939
Measured b_{sp} ($M\,m^{-1}$)	48.14	33.20	6.07	205.65	939
Derived b_{abs} ($M\,m^{-1}$)	4.85	3.31	0.79	23.00	939

measurements, fine particle scattering estimates using DMA data are compared to measured dry fine particle scattering. Recall that the nephelometers were fitted with a 2.5 μm cyclone inlet. Therefore, aerosol mixing characteristics and composition below 2.5 μm must be estimated. SEM data (Hand et al., 2005) clearly suggest that nearly all particles are internally mixed; however, the TDMA aerosol growth measurements of 0.1 and 0.2 μm particles reported by Carrico et al. (2005) show that in most cases there are two modes: more and less hygroscopic. The growth associated with the more hygroscopic mode was still substantially less than a pure inorganic salt, implying a mixed state. The DMA-derived number size distribution data of "dry" particles typically showed a bimodal volume size distribution with a fine mode from about 0.1–0.9 μm. MOUDI data (Malm et al., 2005) show that sulfates and ammonium were predominantly found in the fine mode, while other inorganic species were in size ranges greater than about 0.9 μm. Furthermore, in the fine mode there was sufficient ammonium to fully neutralize sulfate ions. Finally, nitrate <2.5 μm was typically associated with the fine tail of a coarse sodium nitrate mode.

Therefore, one internally mixed mode, externally mixed from two externally mixed coarse modes, was assumed: a fine mode (0.1–0.9 μm) of internally mixed carbonaceous material and ammonium sulfate, and second and third modes consisting of sodium nitrate and dust. It is further assumed that each particle within the size range of 0.1–0.9 μm has the same fractional contribution of sulfate and OMC components. This could be a limiting assumption when attempting to model aerosol growth and associated scattering as a function of RH.

The index of refraction for "soot" or elemental carbon as reported in the literature (Fuller et al., 1999) varies from $1.25+i0.25$ to $2.0+i1.0$ with a median value of $1.8-i0.5$ as reported by Twitty and Weinman (1971). It is this value that was used to estimate the volume-weighted index of refraction of the mixed mode. Indexes of refraction for other species are presented in Table 4.

MIE theory calculations of scattering and absorption assuming spherical particles and the above mixing assumptions are summarized in Table 3 and a scatter plot of measured and modeled scattering is presented in Fig. 2. Also presented in Table 3 are the mixed-state real and imaginary components of the index of refraction, mass scattering and absorption efficiencies, and measured scattering. Notice that the dry mass scattering efficiencies have values that approach $6\,m^2\,g^{-1}$. A regression with measured and DMA-derived scattering as the dependent and independent variables, respectively, yields an R^2 of 0.99, a intercept of $1.47\pm0.23\,Mm^{-1}$ and slope of 0.96 ± 0.004, suggesting a small 4% multiplicative bias between measured and calculated. The estimated uncertainty of the nephelometer is 5%.

7. Comparison of theoretical and measured estimates of *f*(RH)

In an effort to assess the particle growth of organic mass as a function of RH, the f(RH) function was modeled and compared to measured f(RH) values. The strategy taken was to model aerosol growth and f(RH) assuming only inorganics are hygroscopic and compare the modeled f(RH) to measurements of f(RH). Any measured growth beyond that which is predicted with

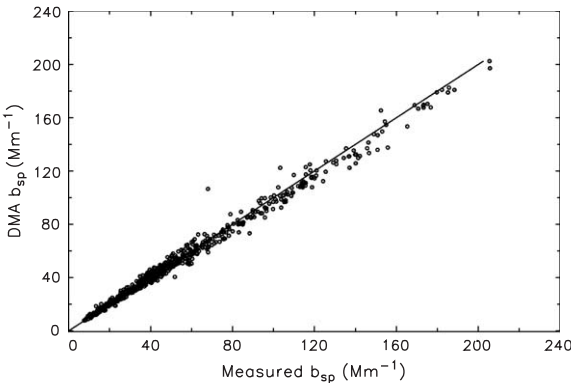

Fig. 2. Scatter plot of measured and modeled aerosol scattering <2.5 μm.

Table 4
Summary of the index of refraction and densities used for modeling scattering and absorption from DMA number size distributions

Species	Density ($g\,cm^{-3}$)	Index of refraction
$(NH_4)_2SO_4$	1.76 (Tang, 1996)	1.53 (Tang, 1996)
Organic carbon	1.4 (Dick et al., 2000)	1.55 (Stelson, 1990)
Elemental carbon	2.0 (Seinfeld and Pandis, 1998)	1.8–0.5 (Twitty and Weinman, 1971)
$NaNO_3$	2.261 (Tang, 1996)	1.59 (Tang, 1996)
Soil	4 (Based on values reported in Hand and Kreidenweis, 2002)	2 (Based on values reported in Hand and Kreidenweis, 2002)

the inorganics-only hygroscopicity assumption can be attributed to organics.

7.1. Measurements of $f(RH)$

Figs. 3–6 show representative f(RH) curves as gray dots along with associated estimated uncertainty bars. The f(RH) curve is based on a five-point running average of data collected every 2 min, while the error bars are plotted every tenth data point. The uncertainty of $f(\mathrm{RH}) = b_{\mathrm{scat}}(\mathrm{RH})/b_{\mathrm{scat,dry}}$ is based on an uncertainty in the nephelometer readings of 5%, while the uncertainty in RH includes an RH measurement error of ± 1 plus the uncertainty in nephelometer sampling chamber RH. Sampling chamber RH uncertainty is associated with the difference between the temperature where the RH measurement is made at the outlet of the nephelometer and actual temperature inside the nephelometer chamber. This difference was approximated by measuring the temperature of the air stream at the inlet and outlet of the nephelometer. Typically, the temperature difference was less than 0.5 °C.

On a small subset of the 52 days, the deliquescent and crystallization branches of the growth curve were measured and hysteresis was usually observed. However, on the days when organic mass concentrations were highest, f(RH) curves were continuous with little to no hysteresis. The emphasis of this analysis will be on the deliquescent f(RH) branch because it was measured on every day the instrument was operated and therefore offers a more complete data set.

Table 5 summarizes the measurements as well as the theoretical estimates of f(RH) that will be discussed in the next section, while Table 6 presents a statistical summary of the average $\mathrm{OMC}/(\mathrm{NH_4})_2(\mathrm{SO_4})$ ratios. Fig. 6 shows $f(85 \leqslant \mathrm{RH} < 90)$ plotted against $\mathrm{OMC}/(\mathrm{NH_4})_2(\mathrm{SO_4})$. There were 29 days when all the measurements required to model f(RH) were present and therefore the analysis is limited to those time periods. The maximum measured $f(90 \leqslant \mathrm{RH} < 95)$ during this study was 2.29 while the minimum was 1.25. In similar studies at Great Smoky Mountains (Malm et al., 2000), Grand Canyon (Malm and Day, 2001), and Big Bend national parks (Malm et al., 2003), the maximum f(RH) was in the 4–5 range while minimums were near 2. The $\mathrm{OMC}/(\mathrm{NH_4})_2(\mathrm{SO_4})$ ratios were on the average, depending on the time the measurement was made, between 4 and 6 with minimums being about 0.5

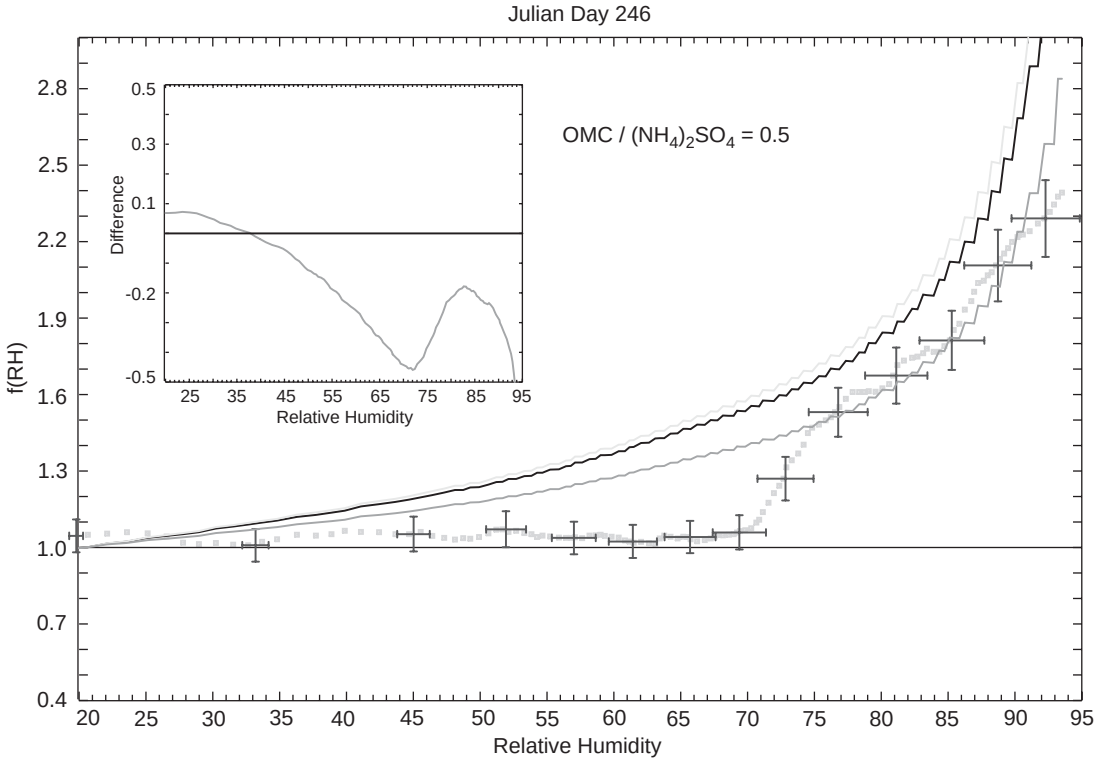

Fig. 3. Measured and modeled f(RH) as a function of relative humidity. Also shown is the difference between measured and modeled f(RH) and the average $\mathrm{OMC}/(\mathrm{NH_4})_2(\mathrm{SO_4})$ ratio during the sampling period. The gray dots are the measured f(RH) curve, while the three solid lines correspond to modeled best estimate and upper and lower bounds of the best estimate.

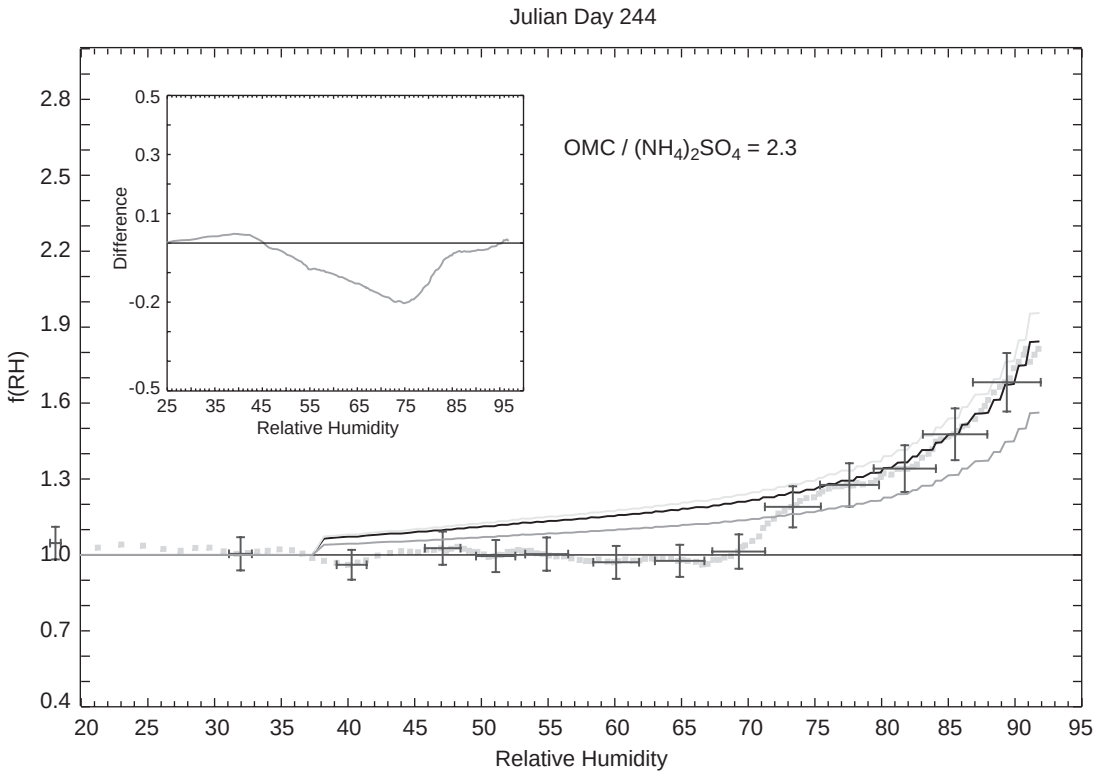

Fig. 4. Measured and modeled f(RH) as a function of relative humidity. Also shown is the difference between measured and modeled f(RH) and the average OMC/$(NH_4)_2(SO_4)$ ratio during the sampling period. The gray dots are the measured f(RH) curve, while the three solid lines correspond to modeled best estimate and upper and lower bounds of the best estimate.

(ammonium sulfate concentrations were twice that of organics) and maximums near 20 (organic mass concentrations were 20 times larger than ammonium sulfate).

Fig. 7 highlights how $f(85<\mathrm{RH}<90)$ varied as the OMC/$(NH_4)_2(SO_4)$ ratio changed. As the OMC/$(NH_4)_2(SO_4)$ ratio increased from a low of 0.57 to 11.15, the $f(85\leqslant\mathrm{RH}<90)$ systematically decreased from about 2 to <1.2. Fig. 7 clearly shows that as organic mass increased, the $f(85\leqslant\mathrm{RH}<90)$, or aerosol growth as a function of RH, decreased. The $f(85\leqslant\mathrm{RH}<90)$ asymptotically approached something near 1.1, implying that the f(RH) associated with organics is small, possibly on the order of 1.1 or less. Carrico et al. (2005) also found an inverse relationship between OMC and D/D_o as measured by a TDMA. They found that D/D_o approached about 1.1 at RH = 80% as the OMC/ionic mass ratio exceeded 10. Virkkula et al. (1999) found a similar observation in a laboratory experiment when coating ammonium sulfate particles with an organic layer. They state that growth, D/D_o, was not proportional to the organic layer thickness but decreased with increasing organic volume fraction and that a pure organic aerosol, formed by oxidation of terpenes, had a growth factor of approximately 1.1. However, it is pointed out that a D/D_o of 1.1 would correspond to an f(RH) of approximately 1.2, which is somewhat higher than that suggested by the data presented in Fig. 7.

7.2. Modeled $f(RH)$

In addition to the assumptions for modeling aerosol scattering discussed above, assumptions concerning aerosol growth as a function of RH must be made. An estimation of ammonium sulfate growth (D/D_o) was calculated using the AIM (Clegg et al., 1998b) equilibrium model over a range of 10–95% RH. The growth of the internally mixed carbon–sulfate aerosol was then estimated using Zdanovskii–Stokes–Robinson (ZSR) (Saxena and Peterson, 1981) assumptions and the aerosol densities presented in Table 4. ZSR assumptions imply that the amount of water a hygroscopic component brings into a mixture at some RH is equal to the amount of water it would have in a binary solution in equilibrium at the same RH.

Upper and lower bounds of f(RH) were modeled by assuming that all species concentrations were 10%

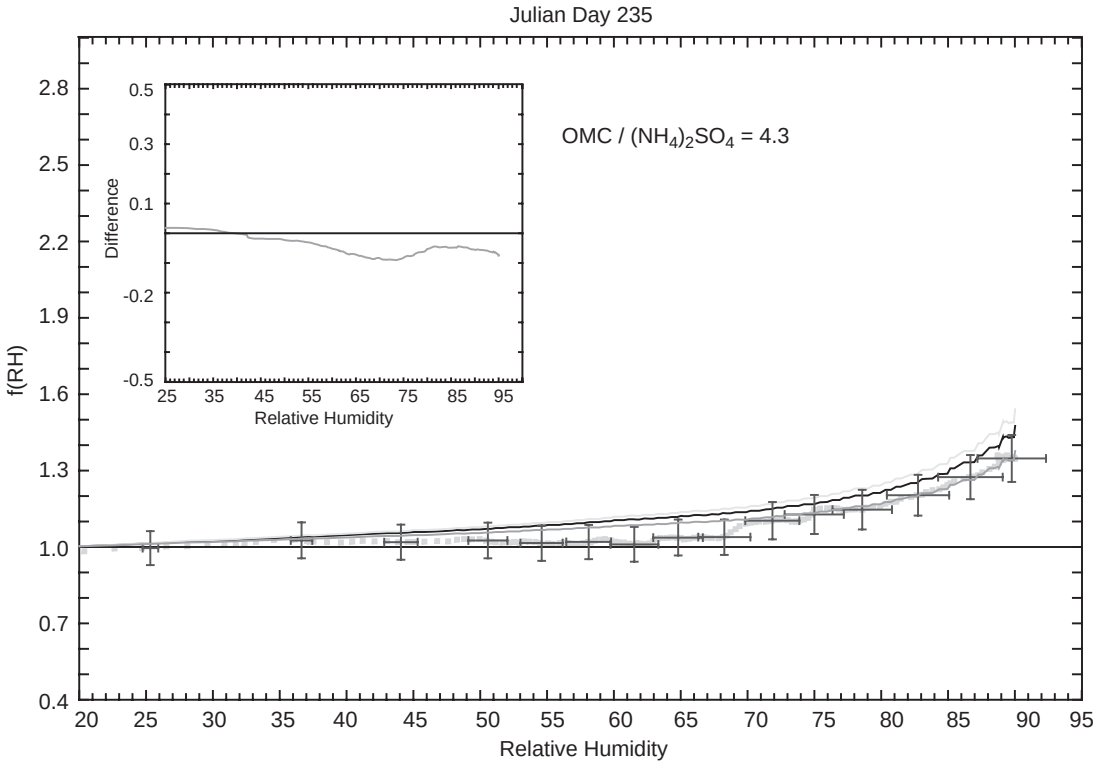

Fig. 5. Measured and modeled f(RH) as a function of relative humidity. Also shown is the difference between measured and modeled f(RH) and the average OMC/$(NH_4)_2(SO_4)$ ratio during the sampling period. The gray dots are the measured f(RH) curve, while the three solid lines correspond to modeled best estimate and upper and lower bounds of the best estimate.

higher or 10% lower than reported and that all or none of the coarse mass scattering was measured. The coarse mass variability was considered because of the "soft" cyclone 2.5 μm cutpoint that is near the peak, or maximum, of the coarse mass fraction size distribution. No uncertainty in index of refraction and density was assumed.

In addition to the four measured f(RH) curves shown in Figs. 3–6 are the corresponding modeled best estimate curves. Lower and upper bound modeled f(RH) curves are also presented. The insets are plots of the difference between the measured and best estimate f(RH) curves. Table 5 presents a statistical summary of measured, modeled, and the difference between measured and modeled f(RH) values as a function of RH.

The four curves correspond to OMC/$(NH_4)_2(SO_4)$ average ratios that vary from a low of 0.5 to 10.5. Note that this ratio can vary substantially over the course of the 2 or 3 h that it takes to carry out an f(RH) scan. Figs. 3 and 4 clearly show deliquescence occurring around 70%. Figs. 5 and 6 show hints of deliquescence in the same RH range; however, the change in f(RH) at the deliquescence point is well within the uncertainty of the measurement. Because the metastable D/D_o growth curve was used in the modeled f(RH), one would only expect measurements and estimated f(RH) curves to agree above the deliquescence point.

Model comparisons to measurements shown in Figs. 3–5 are typical of days when the OMC/$(NH_4)_2(SO_4)$ ratio is less than about 4 in that the best estimate f(RH) curve is either slightly greater or equal to the measured f(RH) curve, with the lower estimate falling within the error bounds of the measurement. Fig. 3 shows a worst-case comparison where the modeled curve above 75% is 0.2–0.5 greater than measured. Differences between measured and modeled f(RH) as large as these suggest that the mixing assumption of a constant OMC to $(NH_4)_2SO_4$ ratio for all sizes <1.0 μm is likely not correct. Apparently, the sulfates and organic mass size distributions differ such that sulfates grow into a more efficient size than implied by the uniform mixing assumption.

Fig. 6 is typical of measured/modeled comparisons when organic mass dominated the fine mass concentration (OMC/$(NH_4)_2(SO_4)$ above about 10). In these sampling periods, the measured f(RH) curve was always slightly more than modeled but within the uncertainty bounds of the analysis. The contribution of organics to

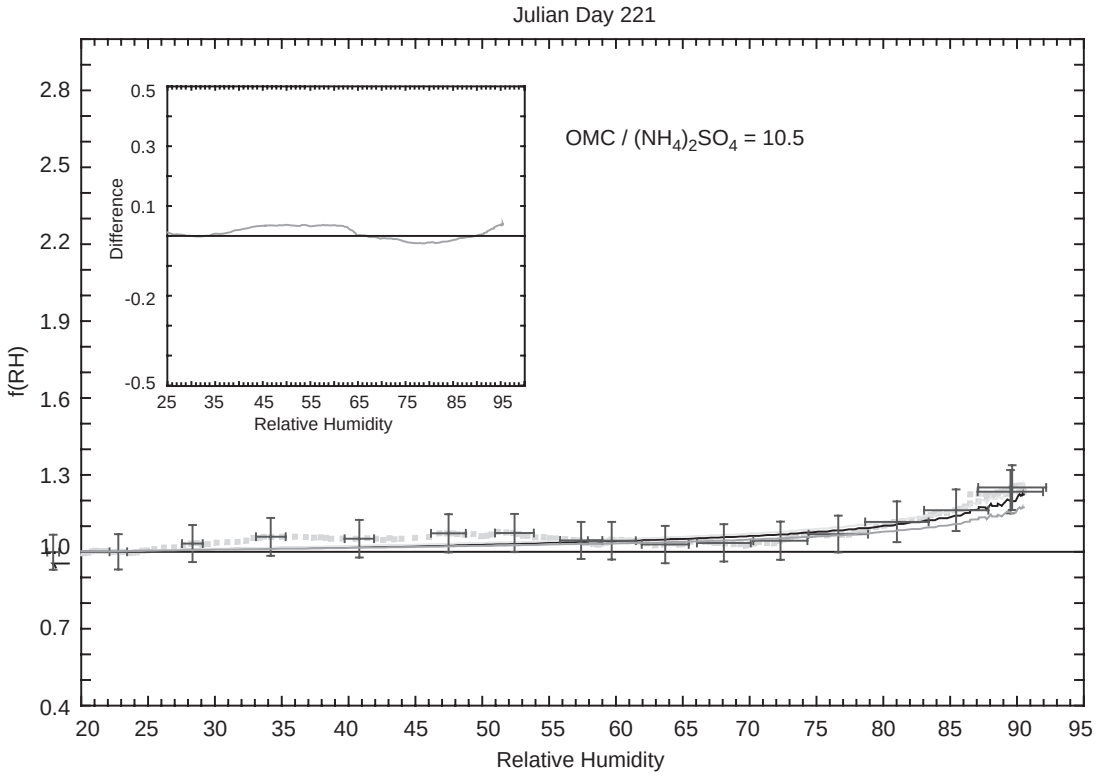

Fig. 6. Measured and modeled f(RH) as a function of relative humidity. Also shown is the difference between measured and modeled f(RH) and the average OMC/$(NH_4)_2(SO_4)$ ratio during the sampling period. The gray dots are the measured f(RH) curve, while the three solid lines correspond to modeled best estimate and upper and lower bounds of the best estimate.

Table 5
Summary of measured and theoretically estimated f(RH) and the difference between measured and modeled (measured–modeled) f(RH)

RH	Measured f(RH)	Std. Dev.	Estimated f(RH)	Std. Dev.	Difference	Minimum	Maximum	N
10–15	1.00	0.01	1.00	0.01	0.007	0.98	1.02	26
15–20	1.01	0.03	1.00	0.00	0.012	0.96	1.10	27
20–25	1.02	0.04	1.00	0.00	0.009	0.95	1.17	29
25–30	1.03	0.04	1.01	0.01	0.015	0.97	1.15	29
30–35	1.03	0.04	1.02	0.02	0.011	0.99	1.19	29
35–40	1.04	0.05	1.03	0.03	0.008	0.98	1.25	29
40–45	1.05	0.05	1.04	0.04	0.001	0.99	1.23	29
45–50	1.06	0.05	1.05	0.04	0.000	1.00	1.24	29
50–55	1.06	0.05	1.07	0.05	−0.013	0.99	1.20	29
55–60	1.06	0.05	1.08	0.07	−0.023	0.98	1.21	29
60–65	1.06	0.05	1.09	0.09	−0.035	0.97	1.19	29
65–70	1.07	0.05	1.12	0.10	−0.048	0.97	1.18	29
70–75	1.12	0.07	1.15	0.13	−0.029	1.00	1.32	29
75–80	1.19	0.12	1.20	0.16	−0.006	1.07	1.56	27
80–85	1.26	0.15	1.27	0.20	−0.010	1.13	1.73	26
85–90	1.37	0.20	1.38	0.27	−0.006	1.15	2.01	21
90–95	1.53	0.30	1.61	0.49	−0.045	1.25	2.29	14

Table 6
Summary of the average OMC/$(NH_4)_2(SO_4)$ ratio for each of the RH ranges at which f(RH) was measured and modeled

RH	Average OMC/$(NH_4)_2(SO_4)$	Std. Dev.	Minimum	Maximum
10–15	6.00	3.81	0.59	16.00
15–20	6.01	4.42	0.49	19.72
20–25	6.04	4.35	0.48	19.23
25–30	5.88	4.22	0.48	18.78
30–35	6.06	4.23	0.47	18.73
35–40	5.93	4.13	0.46	18.22
40–45	5.91	4.01	0.45	17.09
45–50	5.97	4.00	0.44	16.28
50–55	6.03	3.86	0.43	14.82
55–60	6.04	3.78	0.43	14.86
60–65	5.82	3.77	0.45	14.49
65–70	5.50	3.64	0.46	14.24
70–75	5.22	3.36	0.50	13.53
75–80	5.05	3.34	0.53	13.68
80–85	4.73	3.26	0.56	13.54
85–90	4.66	2.63	0.57	11.15
90–95	4.25	2.40	0.58	9.15

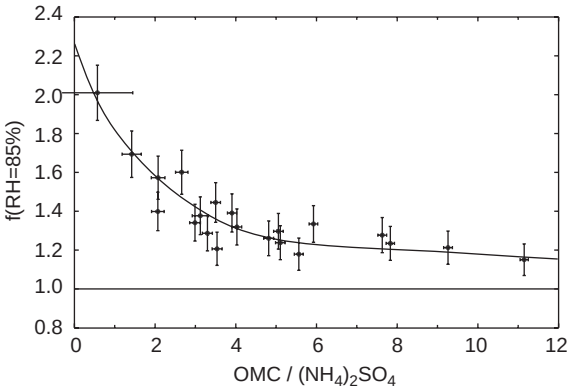

Fig. 7. Plot of $f(80<RH<95)$ as a function of OMC/$(NH_4)_2SO_4$. As organic mass concentrations increase, the hygroscopicity of the aerosol decreases.

the f(RH) at 85–90% RH would not be more than about 1.1, implying a D/D_o associated with organics of not more than about 1.05. On the average, Table 5 shows that in the 70–90% RH range, modeled and measured f(RH) are within about 0.01 of each other with measurements being slightly greater than modeled.

8. Summary

Objectives of the Yosemite Aerosol Characterization Study included characterizing the physical, chemical, and optical properties of a carbon-dominated aerosol, including the ratio of total organic matter weight to organic carbon, organic mass scattering efficiencies, and the hygroscopic characteristics of a carbon-laden ambient aerosol. The study was conducted during July, August, and the first week of September at Turtleback Dome on the south rim of the entrance to Yosemite Valley. This analysis focused on assessing the hygroscopic characteristics, as represented by $f(RH) = b_{scat}(RH)/b_{scat}(RH_{min})$ measurements, of an ambient aerosol that was dominated by organic mass concentrations that at times reached over 85% of gravimetric fine mass.

Analyses of the MOUDI mass size distribution data showed that, on the average, ionic species in the fine mode (0.0–2.5 μm) are made up of primarily ammonium sulfate with about 6% ammonium nitrate and 2% sodium chloride. It was further shown that fine nitrate was actually the fine tail of coarse mode nitrate that was typically in the form of $NaNO_3$. The coarse mode ionic mass is primarily in the form of $NaNO_3$, NaCl, and soil-related nitrate products. Fine mass closure was achieved with an organic mass to organic carbon ratio of 1.8 rather than the more typically used 1.4. On an average basis, OMC made up 69% of the mass, while ammonium sulfate was a distant second at 18%. All other species concentrations contributed to fine mass at <6%. Based solely on optical measurements, these aerosol mass concentrations translated into an ambient extinction apportionment of 75% dry fine particle scattering, 6% coarse particle scattering, 14% coarse and fine absorption, and 5% scattering due to absorbed water.

MIE theory calculations of fine particle scattering and absorption were modeled assuming spherical particles and mixing assumptions of an internally mixed mode of ammonium sulfate and organics externally mixed from fine soil and sodium nitrate. The volume-weighted average real part of the index of refraction was 1.56, while the average complex component was 0.02. The calculations yielded an average mass scattering and an absorption efficiency of 4.5 and $0.46\,m^2\,g^{-1}$, respectively, with mass scattering efficiencies nearing $6.0\,m^2\,g^{-1}$ during time periods with the highest organic mass concentrations.

In general, measurements of f(RH) showed that as OMC increased, f(RH) decreased. As the OMC/$(NH_4)_2(SO_4)$ ratio increased from a low of 0.57 to 11.15, the $f(85\leqslant RH<90)$ systematically decreased from about 2.0 to <1.2. $f(85\leqslant RH<90)$ asymptotically approached something near 1.1, implying that the f(RH) associated with organics is small, possibly on the order of 1.1 or less. Furthermore, the f(RH) function was modeled and compared to measured f(RH) values. The strategy taken was to model aerosol growth and f(RH) assuming only inorganics are hygroscopic and to compare the modeled f(RH) to measurements of f(RH). Any measured growth beyond that which is predicted

with the inorganics-only hygroscopicity assumption can be attributed to organics. On days when the OMC/$(NH_4)_2(SO_4)$ is less than about 4, the best estimate modeled f(RH) curve is either slightly greater or equal to the measured f(RH) curve, with the lower estimate falling within the error bounds of the measurement. When OMC/$(NH_4)_2(SO_4)$ ratios were above about 10, the measured f(RH) curve was always slightly more than modeled but within the uncertainty bounds of the analysis. In these sampling periods, the contribution of organics to the f(RH) at 85–90% RH would not be more than about 1.1, implying a D/D_o associated with organics of not more than about 1.05. On the average, in the 70–90% RH range, modeled and measured f(RH) are within about 0.01 of each other with measurements being slightly greater than modeled.

Disclaimer. The assumptions, findings, conclusions, judgments, and views presented herein are those of the authors and should not be interpreted as necessarily representing the National Park Service policies.

References

Ansari, A.S., Pandis, S.N., 2000. Water absorption by secondary organic aerosol and its effect on inorganic aerosol behavior. Environmental Science and Technology 34, 71–77.

Armendariz, A.J., Leith, D., 2002. Concentration measurement and counting efficiency for the aerodynamic particle sizer 3320. Journal of Aerosol Science 33, 133–148.

Brooks, S.D., DeMott, P.J., Kreidenweis, S.M., 2004. Water uptake by particles containing humic materials and mixtures of humic materials with ammonium sulfate. Atmospheric Environment 38, 1859–1868.

Busch, B., Kandler, K., Schutz, L., Newsuss, C., 2002. Hygroscopic properties and water-soluble volume fraction of atmospheric particles in the diameter range from 50 nm to 3.8 mu during LACE 98. Journal of Geophysical Research—Atmospheres 107 (D21) (Art. No. 8119).

Carrico, C.M., Kreidenweis, S.M., Malm, W.C., Day, D.E., Lee, T., Carrillo, J., McMeeking, G.R., Collett Jr., J.L., 2005. Hygroscopic growth behavior of a carbon dominated aerosol in Yosemite National Park. Atmospheric Environment 39 (8), 1393–1404.

Chan, T., Lippman, M., 1977. Particle collection efficiencies of air sampling cyclones: an empirical theory. Environmental Science and Technology 11, 377–382.

Chow, J.C., Watson, J.G., Pritchett, L.C., Pierson, W.R., Frazier, C.A., Purcell, R.G., 1993. The DRI thermal/optical reflectance carbon analysis system: description, evaluation, and applications in US air quality studies. Atmospheric Environment 27A (8), 1185–1201.

Clegg, S.L., Brimblecombe, P., Wexler, A.S., 1998a. A thermodynamic model of the system H^+–NH_4^+–SO_4^{2-}–NO_3^-–H_2O at tropospheric temperatures. Journal of Physical Chemistry 102A, 2137–2154.

Clegg, S.L., Brimblecombe, P., Wexler, A.S., 1998b. A thermodynamic model of the system H^+–NH_4^+–Na^+–SO_4^{2-}–NO_3^-–Cl^-–H_2O at 298.15 K. Journal of Physical Chemistry 102A, 2155–2171.

Cocker, D.R., Whitlock, N.E., Flagan, R.C., Seinfeld, J.H., 2001. Hygroscopic properties of Pasadena, California aerosol. Aerosol Science and Technology 35 (2), 637–647.

Covert, D.S., Waggoner, A.P., Weiss, R.E., Ahlquist, N.C., Charlson, R.J., 1979. Atmospheric aerosols, humidity and visibility. In: Hidy, G.M., Mueller, P.K., Grosjean, D., Appel, B.R., Weslowski, J.J. (Eds.), Character and Origins of Smog Aerosols. Wiley, New York, pp. 559–581.

Day, D.E., Malm, W.C., 2001. Aerosol light scattering measurements as a function of relative humidity: a comparison between measurements made at three different sites. Atmospheric Environment 35, 5169–5176.

Day, D.E., Malm, W.C., Kreidenweis, S.M., 2000. Aerosol light scattering measurements as a function of relative humidity. Journal of the Air and Waste Management Association 50, 710–716.

Dick, W.D., Saxena, P., McMurry, P.H., 2000. Estimation of water uptake by organic compounds in submicron aerosols measured during the Southeastern Aerosol and Visibility Study. Journal of Geophysical Research—Atmospheres 105, 1471–1479.

Dietrich, L., Molenar, J.V., Faust, J.F., 1989. Transmissometer extinction measurements in an urban environment. In: Mathai, C.V. (Ed.), Visibility and Fine Particles. Air and Waste Management Association, Pittsburgh, PA, pp. 374–383.

Fuller, K.A., Malm, W.C., Kreidenweis, S.M., 1999. Effects of mixing on extinction by carbonaceous particles. Journal of Geophysical Research—Atmospheres 104, 15941–15954.

Gysel, M., Weingartner, E., Nyeki, S., Paulsen, D., Baltensperger, U., Galambos, I., Kiss, G., 2004. Hygroscopic properties of water-soluble matter and humic-like organics in atmospheric fine aerosol. Atmospheric Chemistry and Physics 4, 35–50.

Hand, J.L., Kreidenweis, S.M., 2002. A new method for retrieving particle refractive index and effective density from aerosol size distribution data. Aerosol Science and Technology 36, 1012–1026.

Hand, J.L., Kreidenweis, S.M., Sherman, D.E., Collett Jr., J.L., Hering, S.V., Day, D.E., Malm, W.C., 2002. Aerosol size distributions and visibility estimates during the Big Bend regional aerosol visibility and observational study (BRAVO). Atmospheric Environment 36, 5043–5055.

Hand, J.L., Malm, W.C., Day, D., Lee, T., Carrico, C., Carrillo, J., Collett Jr., J., Laskin, A., Wang, C., Cowin, J.P., Iedema, M.J., 2005. Optical, physical and chemical properties of tar balls during the Yosemite Aerosol Characterization Study. Journal of Geophysical Research, 2004JD005728.

Hansen, A.D.A., Rosen, H., Novakov, T., 1984. The aethalometer—an instrument for the real-time measurement of optical-absorption by aerosol-particles. Science of the Total Environment 36, 191–196.

Hering, S.V., McMurry, P.H., 1991. Optical counter response to monodisperse atmospheric aerosols. Atmospheric Environment Part A—General Topics 25, 463–468.

Kim, Y.P., Seinfeld, J.H., Saxena, P., 1993. Atmospheric gas-aerosol equilibrium. 2. Analysis of common approximations and activity-coefficient calculation methods. Aerosol Science and Technology 19 (2), 182–198.

Knutson, E.O., Lioy, P.J., 1989. Measurement and presentation of aerosol size distributions. In: Hering, S.V. (Ed.), Air Sampling Instruments for Evaluation of Atmospheric Contaminants, 7th ed. American Conference of Governmental Industrial Hygienists, Cincinnati, OH, pp. 59–71.

Laskin, A., Iedema, M.J., Cowin, J.P., 2003. Time-resolved aerosol collector for CCSEM/EDX single-particle analysis. Aerosol Science and Technology 37, 246–260.

Lee, T., Kreidenweis, S.M., Collett Jr., J.L., 2004. Aerosol ion characteristics during the Big Bend regional aerosol and visibility observational study. Journal of the Air and Waste Management Association 54, 585–592.

Malm, W.C., Day, D.E., 2001. Estimates of aerosol species scattering characteristics as a function of relative humidity. Atmospheric Environment 35, 2845–2860.

Malm, W.C., Sisler, J.F., Huffman, D., Eldred, R.A., Cahill, T.A., 1994. Spatial and seasonal trends in particle concentration & optical extinction in the US. Journal of Geophysical Research 99, 1347–1370.

Malm, W.C., Day, D.E., Kreidenweis, S.M., 2000. Light scattering characteristics of aerosols as a function of relative humidity: Part I—a comparison of measured scattering and aerosol concentrations using the theoretical models. Journal of the Air and Waste Management Association 50, 686–700.

Malm, W.C., Day, D.E., Kreidenweis, S.M., Collett Jr., J.L., Lee, T., 2003. Humidity dependent optical properties of fine particles during the Big Bend regional aerosol and visibility study (BRAVO). Journal of Geophysical Research 108 (D9) (Art. No. 4279).

Malm, W.C., Day, D.E., Carrico, C., Kreidenweis, S.M., Collett Jr., J.L., McMeeking, G., Lee, T., Carrillo, J., 2005. Inter-comparison and closure calculations using measurements of aerosol species and optical properties during the Yosemite Aerosol Characterization Study. Journal of Geophysical Research 110, doi:10.1029/2004JD005494.

Marple, V.A., Rubow, K.L., Behm, S.M., 1991. A microorifice uniform deposit impactor (MOUDI)—description, calibration, and use. Aerosol Science and Technology 14, 434–446.

McMeeking, G.R., Kreidenweis, S.M., Carrico, C., Lee, T., Collett Jr., J.L., Malm, W.C., 2005. Observations of smoke influenced aerosol during the Yosemite Aerosol Characterization study, Part I: Size distributions and chemical composition. Journal of Geophysical Research 110(D9), doi:10.1029/2004JD005389.

Molenar, J.V., 1997. Analysis of the real world performance of the Optec NGN-2 ambient nephelometers. In: Visual Air Quality: Aerosols and Global Radiation Balance. Air and Waste Management Association, Pittsburgh, pp. 243–265.

Molenar, J.V., Dietrich, D.L., Tree, R.M., 1989. Application of a long range transmissometer to measure the ambient atmospheric extinction coefficient in remote pristine environments. In: Mathai, C.V. (Ed.), Transactions Visibility and Fine Particles. Air and Waste Management Association, Pittsburgh, PA.

Nenes, A., Pandis, S.N., Pilinis, C., 1998. ISORROPIA: a new thermodynamic equilibrium model for multiphase multicomponent inorganic aerosols. Aquatic Geochemistry 4, 123–152.

Orsini, D.A., Ma, Y.L., Sullivan, A., Sierau, B., Baumann, K., Weber, R.J., 2003. Refinements to the particle-into-liquid sampler (PILS) for ground and airborne measurements of water soluble aerosol composition. Atmospheric Environment 37, 1243–1259.

Prenni, A.J., DeMott, P.J., Kreidenweis, S.M., 2003. Water uptake of internally mixed particles containing ammonium sulfate and dicarboxylic acids. Atmospheric Environment 37, 4243–4251.

Rader, D.J., McMurry, P.H., 1986. Application of the tendem differential mobility analyzer to studies of droplet growth or evaporation. Journal of Aerosol Science 17, 001–017.

Rotronic Instrument Corp., 1998. Humidity–Temperature Meteorological Pro, MP-100F, Fact Sheet. Rotronic Instrument Corp., Huntington, NY.

Rupprecht, G., Patashnick, H., Beeson, D.E., Green, R.N., Meyer, M.B., 1995. A new automated monitor for the measurement of particulate carbon in the atmosphere. In: Presented at the Air and Waste Management Association Conference, Particulate Matter: Health and Regulatory Issues, Pittsburgh, PA.

Saxena, P., Peterson, T.W., 1981. Thermodynamics of multicomponent electrolytic aerosols. Journal of Colloid and Interface Science 79, 496–510.

Seinfeld, J.H., Pandis, S.N., 1998. Atmospheric Chemistry and Physics: from Air Pollution to Climate Change. Wiley, New York, pp. 969–971.

Stelson, A.W., 1990. Urban aerosol refractive-index prediction by partial molar refraction approach. Environmental Science and Technology 24, 1676–1679.

Tang, I.N., 1996. Chemical and size effects of hygroscopic aerosols on light scattering coefficients. Journal of Geophysical Research—Atmospheres 101, 19245–19250.

Twitty, J.T., Weinman, J.A., 1971. Radiative properties of carbonaceous aerosols. Journal of Applied Meteorology 10, 725–731.

United States Environmental Protection Agency, 2003. Guidance for Tracking Progress under the Regional Haze Rule. EPA-454/B-03-004, Office of Air Quality Planning and Standards, Research Triangle Park, NC.

Virkkula, A., Van Dingenen, R., Raes, F., Hjorth, J., 1999. Hygroscopic properties of aerosol formed by oxidation of limonene, alpha-pinene, and beta-pinene. Journal of Geophysical Research 104, 3569–3579.